Supplementary Information for: Influence of material stretchability on the equilibrium shape of a Möbius band

David M. Kleiman,[a] Denis F. Hinz,[b] Yoichi Takato,[c] and Eliot Fried*[c]

[a] *Department of Matthematics and Statistics, McGill University Montréal, Québec, Canada H3A 2K6. E-mail: dave.kleiman2@gmail.com*

[b] *Kamstrup A/S, Industrivej 28, Stilling, 8660 Skanderborg, Denmark. E-mail: dfhinz@gmail.com*

[c] *Mathematical Soft Matter Unit, Okinawa Institute of Science and Technology Onna, Okinawa, Japan 904-0495. E-mail: eliot.fried@oist.jp*

1 Discrete approximations of various curvatures

We approximate a rectangular strip of length L and width w by a lattice of equilateral triangles with N points uniformly separated by an equilibrium distance $r_e = r_0$. The piecewise developable mapping described by Sadowsky [1] is then used to bend and twist the strip into a Möbius band (Figure SI.1), which we then employ as the trial configuration for each numerically determined band with aspect ratio a. Each plane strip is discretized with a lattice of equilateral triangles (SI Figure SI.2 (a)). The variable number of points used to discretize the lattice is denoted by N. Further, the variable number of points along the midline is denoted by N_l.

For a discretized curve with point spacing r_0, the discrete curvature $\kappa(i)$ at the i-th point along the curve is given by

$$\kappa(i) = \frac{\pi - \angle(\mathbf{t}(i), \mathbf{t}(i+1))}{r_0}, \tag{SI.1}$$

where $\angle(\mathbf{t}(i), \mathbf{t}(i+1))$ denotes the angle between discrete tangent vectors at the point i, namely the angle at point i between points $i-1$, i, and $i+1$ (see, for example, Belyaev [2]). Similarly the discrete torsion $\tau(i)$ at the i-th point along the curve is given by

$$\tau(i) = \frac{\angle(\mathbf{b}(i), \mathbf{b}(i+1))}{r_0}, \tag{SI.2}$$

where $\angle(\mathbf{b}(i), \mathbf{b}(i+1))$ denotes the angle between the discrete binormals to the curve at points i and $i+1$.

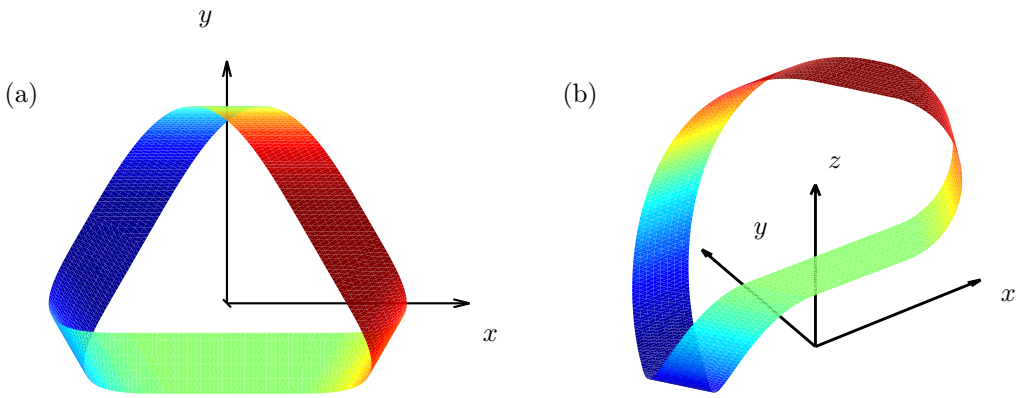

Fig. SI.1: Sadowsky's parametrization of a Möbius band with a developable shape in a Cartesian coordinate system colored by the z-coordinate of each point.

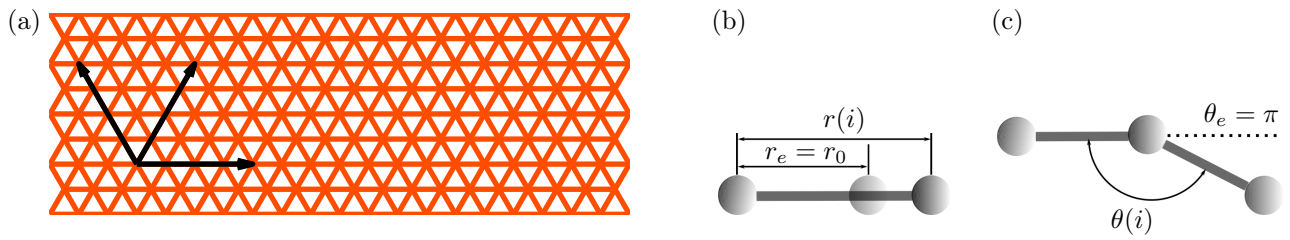

Fig. SI.2: (a) A lattice of equilateral triangles with the three directions of angular and linear springs illustrated. (b) Stretching of an individual linear spring. (c) Bending of an individual angular spring.

To calculate the first and second fundamental forms of surface represented by a discrete triangular lattice, we proceed by analogy to the continuous case (see, for example, do Carmo [3]), but we use vectors between neighboring points on the surface as tangent coordinate vectors. At each point i of the lattice, we determine the discrete mean curvature $H(i)$, the discrete Gaussian curvature $K(i)$, and the discrete principal curvatures $\kappa_1(i)$ and $\kappa_2(i)$ from the first and second fundamental forms.

Let α be the angle between the tangent vector to a curve and the principal direction associated with κ_1. The discrete normal curvature $\kappa_n(i)$ at the i-th point along a curve can then be determined pointwise from the continuous relation

$$\kappa_n = \kappa_1 \cos^2 \alpha + \kappa_2 \sin^2 \alpha. \tag{SI.3}$$

Further, having determined $\kappa(i)$ and $\kappa_n(i)$ from (SI.1) and (SI.3), the magnitude $|\kappa_g(i)|$ of the discrete geodesic curvature $\kappa_g(i)$ can be determined from the continuous relation

$$|\kappa_g| = \sqrt{\kappa^2 - \kappa_n^2}. \tag{SI.4}$$

2 Model validation

To validate our model, we first investigate the influence of the discretization on the equilibrium shape and corresponding energy obtained after minimization. In view of the preceding discussion, we expect that, for each fixed choice of the aspect ratio a, the model approaches a continuum limit as the number N of mesh points is increased. We study the impact of mesh size. To that end, for Möbius bands made from effectively unstretchable materials we consider the convergence of the discrete approximations of the curvature κ and the torsion τ of the midlines but for Möbius bands made from stretchable materials we consider the convergence of Ψ_s, Ψ_b, and Ψ.

Since κ and τ respectively depend on the directions of $\mathbf{t}$ and $\mathbf{n}$, given a point spacing r_0 their convergence does not depend on a length scale. Instead it depends only on the number of points along the midline. If we denote the arclength of the midline by s, the arclength at the i-th point along the midline by s_i, and the number of points along the midline of the band by N_l, then it is most suitable to compare the discrete approximations of the curvature and torsion of the midline for different values of N_l. These approximations are observed to converge to limits as N_l is increased. Results for $a = 4\pi$ are provided in Figure SI.3(a–b). unchanged on increasing N_l from 173 to 347, demonstrating that a choice of N_l in the range $173 < N_l < 347$ produces converged results and that further increasing N_l has negligible impact on the shape of the band (Figure SI.3(a–b)).

For bands made from stretchable materials, we compare Ψ, Ψ_s, and Ψ_b for increasing N_l and different values of γ. All energies show convergence to limiting values (Figure SI.3(c–e)), which is consistent with the previously discussed convergence of the curvature and torsion (Figure SI.3(a–b)) in the case of bands made from effectively unstretchable materials. Note that the value of γ at which energy due to stretching becomes negligible and the unstretchable limit is achieved is not immediately evident. However, for $\gamma = 4.0\pi \cdot 10^6$, Ψ_s is approximately 1% of Ψ, indicating that it is reasonable to conclude that the choice $\gamma = 4.0\pi \cdot 10^6$ provides a very close approximation to unstretchability.

3 Connection between lattice and continuum models

3.1 Bending energy

Sadowsky's [1, 4, 5] work on Möbius bands made from effectively unstretchable materials hinges on a continuum description in which a strip is treated as a surface S endowed with bending-energy density proportional to the

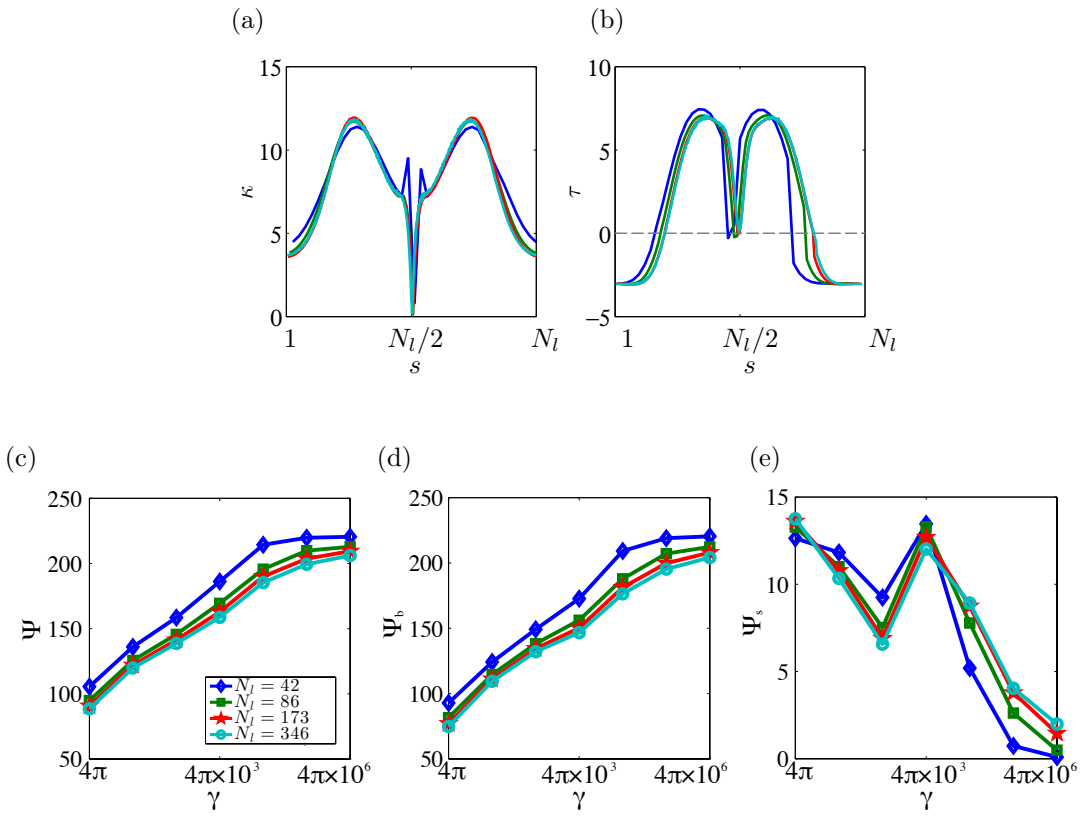

Fig. SI.3: The model shows convergence for increasing number of points along the midline: The (a) curvature κ and (b) torsion τ of the midline for approximately unstretchable bands ($\gamma = 4.0\pi \cdot 10^6$) approach a limiting value for a large number of points along the midline $173 < N_l$. The total energy Ψ (c), stretching energy Ψ_s (d), and Ψ_b (e) converge to a limiting shape corresponding to the continuum limit. Results are shown for $a = 4\pi$.

square of its mean curvature H. By the *Theorema Egregium* of Gauss [6], bending a surface without stretching or shrinking leaves its Gaussian curvature K unchanged. Simultaneous bending and stretching of a surface will, however, generally alter its Gaussian curvature. To model stretchable bands, it is therefore natural to incorporate energetic dependence on Gaussian curvature. In keeping with a quadratic dependence on mean curvature, this amounts to augmenting Sadowsky's bending energy with a term linear in the Gaussian curvature. Granted that the band is free of spontaneous mean curvature, this leads to the Canham–Helfrich bending-energy functional

$$E_{\text{bend}} = \int_S (2\mu H^2 + \bar{\mu} K)\, \mathrm{d}A, \tag{SI.5}$$

involving the bending-energy density

$$\psi_{\text{bend}} = 2\mu H^2 + \bar{\mu} K, \tag{SI.6}$$

where $\mu > 0$ is the splay modulus and $\bar{\mu} < 0$ is the saddle-splay modulus. Importantly, since $K = 0$ for a developable surface, (SI.5) reduces in the unstretchable limit to the functional considered by Sadowsky [1, 4, 5].

Although connections between the Canham–Helfrich functional (SI.5) and triangular lattice parameters have already been established by Seung and Nelson [7] and Schmidt and Fraternali [8], these rely on potentials involving the normals of neighboring triangular cells. Defining the normals to the cells of a triangulation of a nonorientable surface like a Möbius band is problematic. Hence, we use other elementary geometric considerations to establish a connection between (SI.5) and the bending-energy functional

$$E_b = \sum_{i \in S_\theta} U_{\theta i} = \frac{k_\theta}{2} \sum_{i \in S_\theta} (\theta(i) - \pi)^2 \tag{SI.7}$$

of the discrete lattice. We recall that in (SI.7) S_θ is the set of all angular springs.

To determine the effective splay and saddle-splay moduli μ and $\bar{\mu}$ corresponding to the underlying triangular lattice, we first use the definition (SI.1) of the discrete curvature $\kappa(i)$ in the expression for the bending energy E_b.

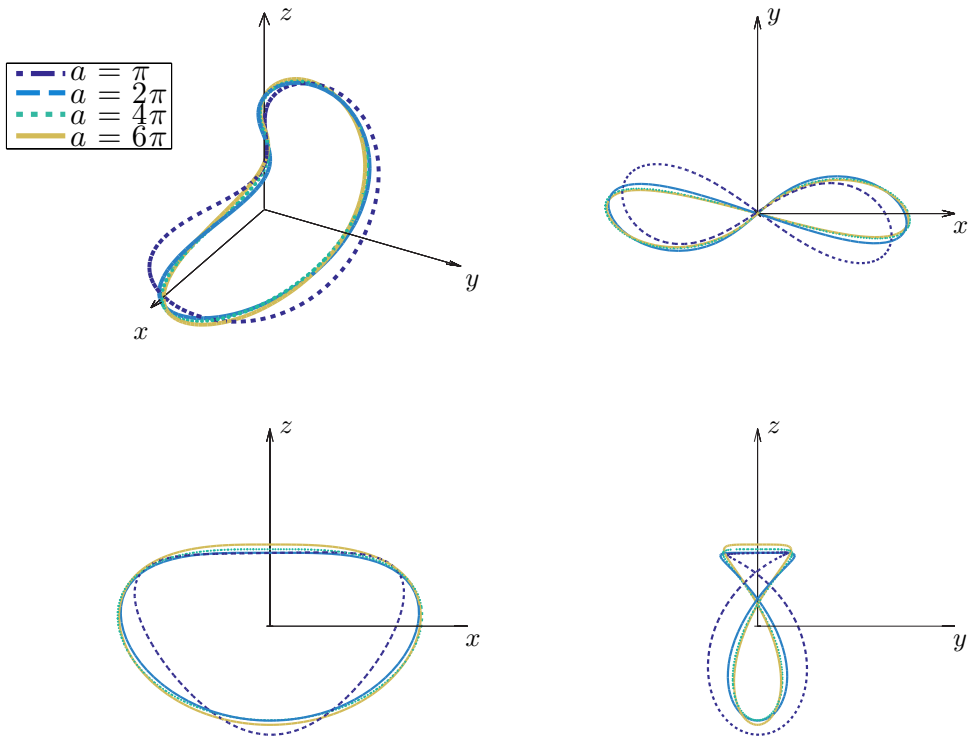

Fig. SI.4: The midline of an approximately unstretchable Möbius band depends on its aspect ratio: Centerlines of equilibrium shapes of general Möbius bands for different values of the aspect ratio a with FvK number γ kept at $4.0\pi \cdot 10^6$ for all aspect ratios. The band is rotated into its main axes.

Taking into account that the lattice is periodic, this yields

$$E_b = \tfrac{1}{2} k_\theta r_0^2 \sum_{i=1}^{N} \sum_{j=1}^{3} (\kappa^{(j)}(i))^2, \tag{SI.8}$$

where r_0 is the distance between lattice points, N is the number of points on the surface, and $k_\theta > 0$ is the lattice modulus associated with bending (E_b in (SI.8) carries the same dimensions as E_{bend} in (SI.5)), $\kappa^{(j)}(i)$ is the curvature of the j-direction lattice line at point i for $j = 1, 2, 3$. Further, letting the angle between the 1-direction lattice line at point i and the first principal direction at point i be $\alpha(i)$, we can use the expressions (SI.3) and (SI.4) for κ_n and κ to write (SI.8) as

$$\begin{aligned} E_b = \tfrac{1}{2} k_\theta r_0^2 \sum_{i=1}^{N} \Bigg(\sum_{j=1}^{3} (\kappa_g^{(j)}(i))^2 + (\kappa_1(i))^2 \left[\cos^4(\alpha(i)) + \cos^4\left(\alpha(i) + \frac{\pi}{3}\right) + \cos^4\left(\alpha(i) + \frac{2\pi}{3}\right) \right] \\ + (\kappa_2(i))^2 \left[\sin^4(\alpha(i)) + \sin^4\left(\alpha(i) + \frac{\pi}{3}\right) + \sin^4\left(\alpha(i) + \frac{2\pi}{3}\right) \right] \Bigg), \end{aligned} \tag{SI.9}$$

where the angle between lattice lines is required to remain equal to $\pi/3$. To enforce this constraint on the angle, we assume the distance between points remains constant. This assumption yields reasonable approximations for small deformations. Further, it implies that lattice lines are geodesics—i.e., $\kappa_g \equiv 0$ along lattice lines. We next use the

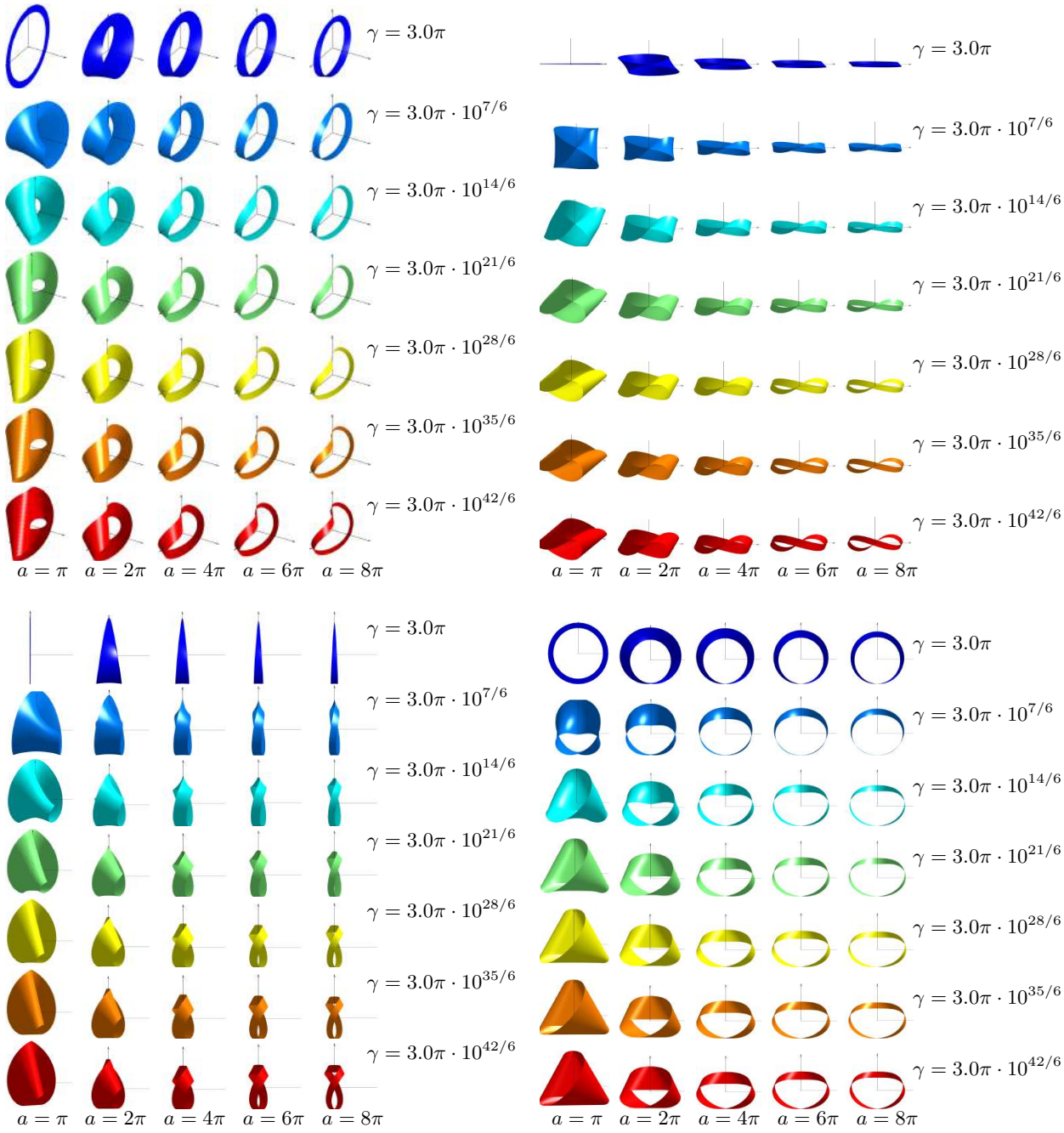

Fig. SI.5: Generalized Möbius bands adopt characteristic equilibrium shapes depending on the in-plane stretchability of the surface and the aspect ratio: Equilibrium shapes of generalized Möbius bands for different values of the aspect ratio a and FvK number γ. Each band is rotated into its main axes.

identities

$$\left.\begin{aligned}
\cos^4\vartheta + \cos^4\left(\vartheta + \frac{\pi}{3}\right) + \cos^4\left(\vartheta + \frac{2\pi}{3}\right) &= \frac{9}{8},\\
\sin^4\vartheta + \sin^4\left(\vartheta + \frac{\pi}{3}\right) + \sin^4\left(\vartheta + \frac{2\pi}{3}\right) &= \frac{9}{8},\\
\cos^2\vartheta + \cos^2\left(\vartheta + \frac{\pi}{3}\right) + \cos^2\left(\vartheta + \frac{2\pi}{3}\right) &= \frac{3}{2},\\
\sin^2\vartheta + \sin^2\left(\vartheta + \frac{\pi}{3}\right) + \sin^2\left(\vartheta + \frac{2\pi}{3}\right) &= \frac{3}{2},
\end{aligned}\right\} \tag{SI.10}$$

(a) $\gamma = 3.0\pi$ $\gamma = 3.0\pi \cdot 10^{7/6}$ $\gamma = 3.0\pi \cdot 10^{14/6}$ $\gamma = 3.0\pi \cdot 10^{21/6}$ $\gamma = 3.0\pi \cdot 10^{28/6}$ $\gamma = 3.0\pi \cdot 10^{35/6}$ $\gamma = 3.0\pi \cdot 10^{42/6}$

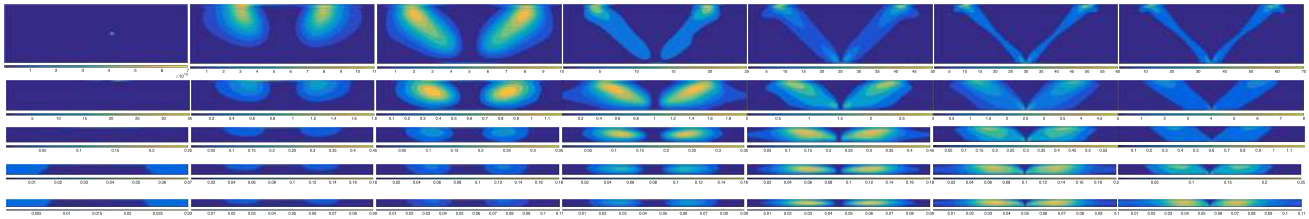

(b) $\gamma = 3.0\pi$ $\gamma = 3.0\pi \cdot 10^{7/6}$ $\gamma = 3.0\pi \cdot 10^{14/6}$ $\gamma = 3.0\pi \cdot 10^{21/6}$ $\gamma = 3.0\pi \cdot 10^{28/6}$ $\gamma = 3.0\pi \cdot 10^{35/6}$ $\gamma = 3.0\pi \cdot 10^{42/6}$

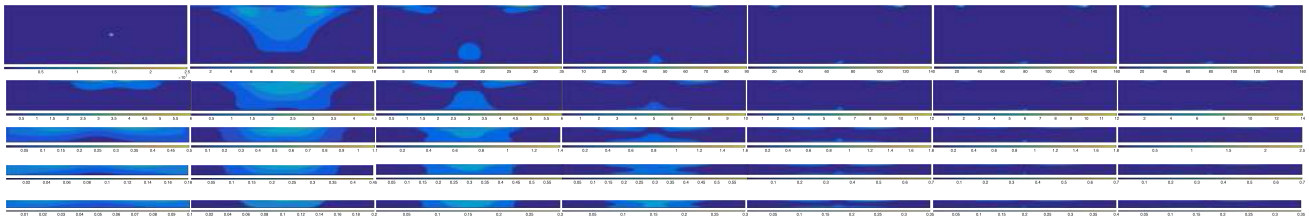

(c) $\gamma = 3.0\pi$ $\gamma = 3.0\pi \cdot 10^{7/6}$ $\gamma = 3.0\pi \cdot 10^{14/6}$ $\gamma = 3.0\pi \cdot 10^{21/6}$ $\gamma = 3.0\pi \cdot 10^{28/6}$ $\gamma = 3.0\pi \cdot 10^{35/6}$ $\gamma = 3.0\pi \cdot 10^{42/6}$

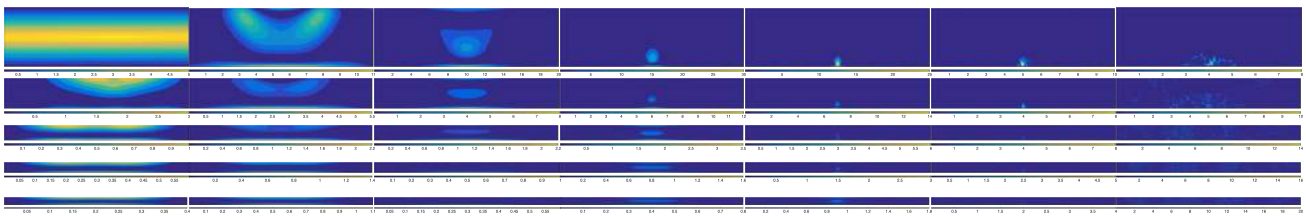

Fig. SI.6: Both mean and Gaussian curvature are more evenly distributed for decreasing FvK number γ: (a) Square H^2 of the mean curvature H, (b) magnitude $|K|$ of the Gaussian curvature, and (c) square ϵ^2 of the strain ϵ of generalized Möbius bands for different values of the aspect ratio a and FvK number γ. The aspect ratio of each contour plot is equal to the aspect ratio of the band it represents. Note the different scales adapted individually to capture the entire range of values.

to reduce (SI.9) to

$$E_b = \frac{k_\theta r_0^2}{2} \sum_{i=1}^{N} \left(\frac{9}{2}(H(i))^2 - \frac{3}{2}K \right), \tag{SI.11}$$

where $H(i)$ and $K(i)$ are the respective discrete mean and Gaussian curvatures at the lattice point i. Finally, a Riemann sum argument yields

$$E_b \approx \sqrt{3} k_\theta \int_S (3H^2 - K)\, \mathrm{d}A \tag{SI.12}$$

for which the corresponding bending-energy density is

$$\psi_{\text{bend}} = \sqrt{3} k_\theta (3H^2 - K). \tag{SI.13}$$

Comparison with (SI.5) yields

$$\mu = \frac{3\sqrt{3} k_\theta}{2} \quad \text{and} \quad \bar{\mu} = -\sqrt{3} k_\theta. \tag{SI.14}$$

To validate the foregoing calculations, we present the example of a plane strip discretized with a lattice mapped isometrically to a helically wrapped strip (Figure SI.2).

Let $\{\mathbf{e}_1, \mathbf{e}_2, \mathbf{e}_3\}$ denote a rectangular Cartesian basis and consider a helix of radius $r > 0$ and pitch $2\pi b > 0$ parametrized by

$$\boldsymbol{\alpha}(t) = r \cos t\, \mathbf{e}_1 + r \sin t\, \mathbf{e}_2 + bt\, \mathbf{e}_3 \tag{SI.15}$$

for $t \in \mathbb{R}$. On eliminating b between the relations

$$\varphi = \arctan\left(\frac{b}{r}\right) \qquad \text{and} \qquad \kappa = \frac{r}{r^2 + b^2} \tag{SI.16}$$

defining the lead angle and curvature of the helix, we obtain

$$\kappa = \frac{\cos^2 \varphi}{r}. \tag{SI.17}$$

If a plane strip approximated by a triangular lattice is wrapped helically around a cylinder, then at any point i, the curve in the j-direction is a helix. Further, letting $\varphi^{(j)}(i)$ be the lead angle of the helix through the point i in the j-direction, it is evident that

$$\varphi^{(3)}(i) = \varphi^{(2)}(i) + \frac{\pi}{3} = \varphi^{(1)}(i) + \frac{2\pi}{3}. \tag{SI.18}$$

Now substituting (SI.18) into (SI.17) yields

$$\left.\begin{aligned} \kappa^{(1)}(i) &= \frac{\cos^2(\varphi^{(1)}(i))}{r}, \\ \kappa^{(2)}(i) &= \frac{\cos^2(\varphi^{(2)}(i) + \frac{\pi}{3})}{r}, \\ \kappa^{(3)}(i) &= \frac{\cos^2(\varphi^{(3)}(i) + \frac{2\pi}{3})}{r}. \end{aligned}\right\} \tag{SI.19}$$

Finally, substituting (SI.19) into (SI.8) yields

$$E_B = \frac{1}{2} k_\theta \frac{r_0^2}{r^2} \sum_{i=1}^{N} \left(\cos^4(\varphi^{(1)}(i)) + \cos^4\left(\varphi^{(1)}(i) + \frac{\pi}{3}\right) + \cos^4\left(\varphi^{(1)}(i) + \frac{2\pi}{3}\right)\right). \tag{SI.20}$$

Reducing, as in the general case, results in

$$E_B = \frac{3\sqrt{3} k_\theta A}{4r^2}. \tag{SI.21}$$

Since $H^2 \equiv 1/4r^2$ for a helically wrapped strip, comparison of (SI.21) with the Canham–Helfrich bending energy functional (SI.5) confirms that

$$\mu = \frac{3\sqrt{3} k_\theta}{2}. \tag{SI.22}$$

Notice that (SI.21) is independent of $\varphi^{(j)}(i)$ and thus of the orientation of the triangular lattice; consistent with the discussion of Vigliotti et al. [9], this assures that the triangular lattice behaves isotropically in bending. Additionally, in the approximately unstretchable, where K is very close to zero, (SI.12) is dominated by the term involving H^2, demonstrating that, for large γ, we approximately minimize the integral of H^2 over the surface. As reported by Sadowsky [1, 4, 5], Mahadevan and Keller [10], and Starostin and van der Heijden [11, 12], this result is consistent with analogous results from continuum theory.

Finally, we can further compare (SI.13) to the bending-energy density

$$D(2H^2 - (1-\nu)K) \tag{SI.23}$$

for a thin plate derived by Keller and Merchant [13] in which D is the bending modulus and ν is the Poisson ratio. To achieve consistency between (SI.13) and (SI.23), the material must have $\nu = 1/3$. In contrast, similar calculations using expressions for μ and $\bar{\mu}$ provided by Seung and Nelson [7] and Schmidt and Fraternali [8] respectively yield $\nu = 0$ and $\nu = -1/3$.

3.2 Stretching energy

Apart from energy due to bending, Möbius bands made from stretchable materials store elastic energy due to in-plane stretching. Using the purely two-dimensional theory of linearized elasticity and neglecting contributions due to shear results in the area stretching-energy functional of the form (Deserno [14])

$$E_{\text{stretch}} = 2\mu_s \int_S \epsilon^2 \, \mathrm{d}A, \tag{SI.24}$$

where $\mu_s > 0$ is the two-dimensional bulk (area) modulus and $\epsilon \approx (J-1)/2 \approx (A/A_0 - 1)/2$ is an approximation for the local in-plane strain, with J being the areal Jacobian determinant and A the current area of an area element

with reference area A_0. (E_{stretch} carries dimensions of energy.) In the present two-dimensional setting, μ_s carries dimensions of energy/length^2. In view of (SI.24), the stretching-energy density is

$$\psi_{\text{stretch}} = 2\mu_s \epsilon^2. \tag{SI.25}$$

We now relate the energy of a discrete set of springs to the continuum expression (SI.24) with two primary objectives: (I) to determine the effective value of μ_s for an equilateral triangular lattice of linear springs, and (II) to verify the isotropy of such a lattice. Stretching energy E_s of a collection of linear springs is given by

$$E_s = \frac{k_l}{2} \sum_{i=1}^{N_s} [(r(i) - r_0)^2], \tag{SI.26}$$

where $k_l > 0$ is the lattice modulus associated with stretching carrying the same dimensions as the two-dimensional bulk modulus μ_s, N_s is the number of linear springs, $r(i)$ is the current length of the i-th spring, and r_0 is the equilibrium length of the springs. Notice that in the discrete setting, pure dilatation amounts to uniform stretching of the lattice. That is, each unit cell stretches (or contracts) into a larger (or smaller) equilateral triangle. The stretching energy of a unit cell in a periodic equilateral triangular lattice is

$$E_{\text{UC}} = \frac{k_l}{4} [(r(1) - r_0)^2 + (r(2) - r_0)^2 + (r(3) - r_0)^2], \tag{SI.27}$$

where $r(1)$, $r(2)$, and $r(3)$ are the lengths of the sides of the unit cells. Notice that the additional factor $1/2$ in (SI.27) accounts for periodicity, namely that each spring is shared by neighboring unit cells. For pure dilatation (uniform stretching), $r(1) = r(2) = r(3) = r$ and (SI.27) reduces to

$$E_{\text{UC}} = \frac{3k_l}{4} (r - r_0)^2. \tag{SI.28}$$

Using the area $A_0 = \sqrt{3} r_0^2/4$ of a unit cell and the magnitude of the pure dilatational strain $\epsilon = (r - r_0)/r_0$ yields

$$E_s = N_{\text{UC}} E_{\text{UC}} = \sqrt{3} k_l \int_S \epsilon^2 \, \mathrm{d}A. \tag{SI.29}$$

Importantly, (SI.29) is the lattice counterpart of (SI.24), and comparison of terms yields the connection

$$\mu_s = \frac{\sqrt{3} k_l}{2} \tag{SI.30}$$

between the effective continuum modulus μ_s and the lattice modulus k_l. Notice that (SI.30) is consistent with a previously established connection between lattice and continuum parameters due to Seung and Nelson [7].

The relationship (SI.30) is valid for periodic lattices. In the special case of one isolated unit cell without neighbors, the factor of $1/2$ in (SI.27) vanishes, and it correspondingly follows that

$$\mu_{s_1} = \sqrt{3} k_l. \tag{SI.31}$$

Further, within the continuum theory, the following approximations hold

$$\text{tr}\,(\epsilon \mathbf{I}) = 3\epsilon \approx J - 1 \approx \frac{A}{A_0} - 1, \tag{SI.32}$$

where J is the areal Jacobian of the deformation and $\mathbf{I}$ is the two-dimensional identity tensor. In view of (SI.32), the expression (SI.29) for E_s can be written as

$$E_s = N_{\text{UC}} E_{\text{UC}} = \frac{k_l N_{\text{UC}} r_0^2}{12} \left(\frac{A}{A_0} - 1 \right)^2. \tag{SI.33}$$

3.3 Numerical results

Consistent with the linearized theory of elasticity, the derivations leading to (SI.14) and (SI.30) are predicated on assuming that the strains and rotations are infinitesimal. We therefore expect deviations from the continuum theory for sufficiently small values of the FvK number γ. For $\gamma \gtrsim 3.0\pi \cdot 10^{35/12}$, we find that the dimensionless bending

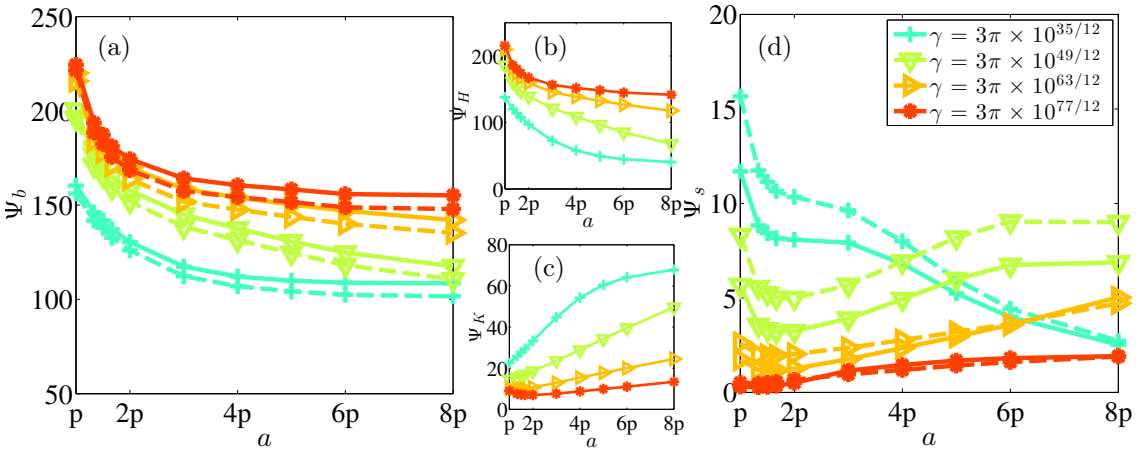

Fig. SI.7: The dimensionless bending energy of the lattice model coincides with the bending energy of the Canham–Helfrich continuum functional using the theoretically determined splay modulus μ and saddle splay modulus $\bar{\mu}$: (a) Dimensionless bending energy of the lattice model (dashed lines) and that from the Canham–Helfrich functional (solid lines). Dimensionless energy contributions to the Canham–Helfrich energy functional from (b) H^2 and (c) K. (d) Dimensionless stretching energy due to dilatation (solid lines) is consistently of lower magnitude than that of the lattice model (dashed lines), but both exhibit the same trend.

energy Ψ_b computed from a suitably normalized version of (SI.11) (Figure SI.7(a) solid lines) and its counterpart for the discrete lattice (SI.7) (Figure SI.7(a) dashed lines) coincide. Importantly, the dimensionless energies agree for both small and large contributions associated with K (Figure SI.7(b–c)), which confirms the expressions (SI.14) for the continuum parameters. For $\gamma \lesssim 3.0\pi \cdot 10^{35/12}$, we observe deviations from the continuum theory for small aspect ratios. This occurs since, as bands approach a self-intersecting shape, the dimensionless continuum functional becomes orders of magnitude larger than the dimensionless lattice energy due to divergent values of H^2 and K near points of self-intersection (not shown).

From Figure SI.7(d), we observe that the dimensionless stretching energy due to dilatation is consistently of lower magnitude than that of the lattice model. This indicates that for thin, stretchable materials capable of supporting shear strain, energy contributions due to in-plane shearing are not negligible when a strip of material is twisted into a Möbius band. As Deserno [14] explains, the Canham–Helfrich theory neglects energy contributions due to shear and describes simple surfaces, like spheres, very well, but might not be suitable to model topologically complex objects such as Möbius bands.

3.4 Numerical validation of the stretching energy

For pure dilatation and assuming periodic boundaries, the total energy E_s of a collection of springs (SI.26) and the energy of a unit cell are related through

$$E_s = N_{\mathrm{UC}} E_{\mathrm{UC}}, \tag{SI.34}$$

where N_{UC} is the number of unit cells. In view of (SI.34) and (SI.24), the effective stretching modulus can be extracted from the value of (SI.26) determined by simulation through

$$\mu_s = \frac{E_s}{2\epsilon^2 N_{\mathrm{UC}} A_0}. \tag{SI.35}$$

By analogy to the various scalings introduced in the main text, using k_l and the reference area $A = N_{\mathrm{UC}} A_0$ to nondimensionalize (SI.34) and (SI.35) yields the dimensionless counterparts

$$\Psi_s = \frac{E_s}{A k_l} = \frac{E_s}{N_{\mathrm{UC}} k_l A_0} \tag{SI.36}$$

and

$$\tilde{\mu}_s = \frac{\mu_s}{k_l} = \frac{E_s}{2\epsilon^2 N_{\mathrm{UC}} A_0 k_l}. \tag{SI.37}$$

In view of (SI.29), the following identifications hold: $E_s = \sqrt{3}\int_S \epsilon^2 \,\mathrm{d}A$, $\tilde{\mu}_s = \sqrt{3}/2$, and $\tilde{\mu}_{s_1} = \sqrt{3}$. To quantify the parameter range in which the plane lattice subject to in-plane pure dilatation behaves linearly elastically, we

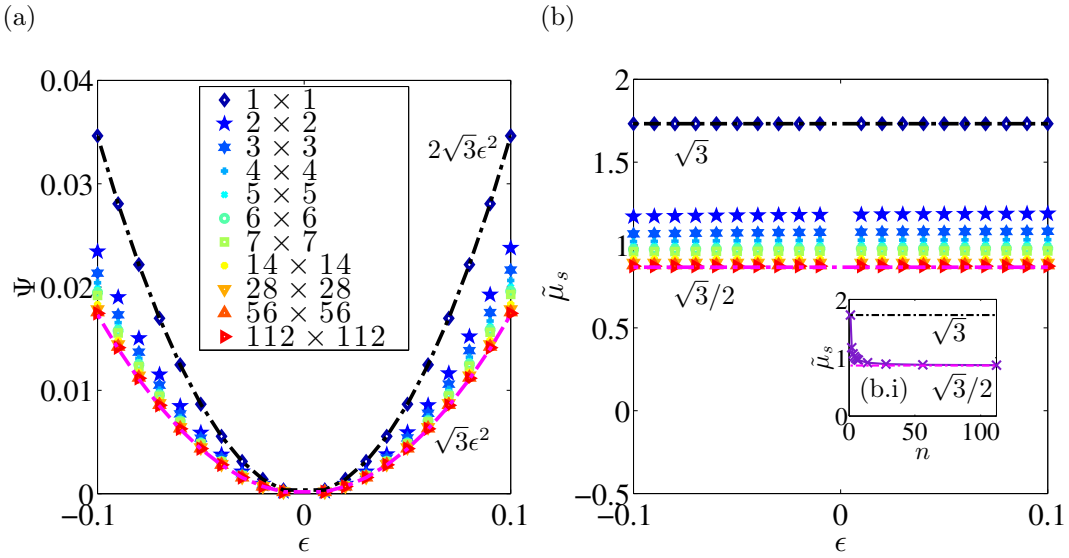

Fig. SI.8: The lattice behaves linearly elastically, and the effective bulk modulus $\tilde{\mu}_s$ converges towards the theoretical prediction: (a) Dimensionless energy Ψ_s as a function of strain ϵ along with the theoretical predictions $\Psi = \sqrt{3}\epsilon^2$ and $\Psi_1 = 2\sqrt{3}\epsilon^2$. (b) Dimensionless effective bulk modulus $\tilde{\mu}_s$ as a function of strain ϵ with the theoretical predictions $\tilde{\mu}_s = \sqrt{3}/2$ and $\tilde{\mu}_{s_1} = \sqrt{3}$. (b.i) Convergence of $\tilde{\mu}_s$ for increasing number of segments n.

measure (SI.37) for different imposed ϵ and different sizes of the lattice (or, equivalently, different N_{UC}). The lattice sizes range from 1×1 to 112×112 triangular unit cells (SI Figure SI.8), and the strains range from $\epsilon = -0.1$ to $\epsilon = 0.1$. The energy is found to converge to the theoretically determined value, with little difference between results obtained for a 14×14 lattice and for a 112×112 lattice.

References

1 M. Sadowsky, *Sitzungsberichte der Preussischen Akademie der Wissenschaften, physikalisch-mathematische Klasse*, 1930, **22**, 412–415.

2 A. G. Belyaev, Proceedings of the Symposium on Singularity Theory and Differential Equations, Feb. 1-4, 1999, Research Institute for Mathematical Sciences, Kyoto University. RIMS Kôkyûroku **1111**:157–164, 1999.

3 M. P. do Carmo, *Differential geometry of curves and surfaces*, Prentice-Hall, Englewood Cliffs, New Jersey, 1976.

4 M. Sadowsky, Proceedings of the 3rd Int Congress of Applied Mechanics, Stockholm, AB. Sveriges Litografiska Tryckerier, Stockholm, 1930, pp. 444–451.

5 M. Sadowsky, *Jahresbericht der Deutschen Mathematiker Vereinigung, (Report on the Annual Conference, Prague, 16–23 Sept., 1929)*, 1930, **39**, 49–51 (2. Abteilung).

6 K. F. Gauss, *Commentationes Societatis Regiae Scientiarum Gottingensis Recentiores*, 1827, **6**, 99–146.

7 H. S. Seung and D. R. Nelson, *Physical Review A*, 1988, **38**, 1005–1018.

8 B. Schmidt and F. Fraternali, *Journal of the Mechanics and Physics of Solids*, 2011, **60**, 172–180.

9 A. Vigliotti, V. S. Deshpande and D. Pasini, *Journal of the Mechanics and Physics of Solids*, 2014, **64**, 44–60.

10 L. Mahadevan and J. B. Keller, *Proceedings of the Royal Society of London Series A, Mathematical, Physical and Engineering Sciences*, 1993, **440**, 149–162.

11 E. L. Starostin and G. H. M. van der Heijden, *Proceedings in Applied Mathematics and Mechanics*, 2007, **7**, 2020115–2020116.

12 E. L. Starostin and G. H. M. van der Heijden, *Nature Materials*, 2007, **6**, 563–567.

13 J. B. Keller and G. J. Merchant, *Journal of Statistical Physics*, 1991, **63**, 1039–1051.

14 M. Deserno, *Chemistry and Physics of Lipids*, 2014.